Figure 3. Generation of chimpanzee iPSCs with the TS12KOS vector. (**a**) Summary of chimpanzee iPSC generation. iPSCs were generated from the blood cells of two chimpanzee individuals with TS12KOS or the conventional SeV vectors. (**b**) Effect of the T lymphocyte stimulation on iPSC generation. Experiments were conducted in triplicate (mean ± SD). *$P<0.01$, PHA versus anti-CD3 antibody or Con A stimulations, Student's t-test. (**c**) Colony morphology and AP staining of iPSCs from stimulated T lymphocytes. (**d**) Phase contrast images, immunofluorescence for pluripotency markers, and alkaline phosphatase (AP) staining of chimpanzee iPSC lines. C101, C201, C205, and C402 are described in **Fig. 3a**. Scale bars, 200 μm. (**e**) RT-PCR analysis of SeV and human ES cell markers. SeV, first RT-PCR for SeV; nested, nested RT-PCR for SeV; 201B7, control human iPSC line; SeV(+), Day 7 SeV-infected human fibroblasts. (**f**) PCR products with primers that can distinguish chimpanzee and human genomes. Chimpanzee PCR products; 782, 472 and 504 bps, Human PCR products; 203, 245, 278 bps. (**g**) Chromosomal analyses of chimpanzee iPSC lines generated with the TS12KOS vector. (**h**) TCR gene recombination. Genes from the chimpanzee iPSC lines were digested with the indicated enzymes and hybridized with the TCR probes by Southern blotting. Arrows indicate the germ bands of TCR genes. HeLa and 201B7: human cell lines, MT4: human T cell line, HSP-239: chimpanzee T cell line.

doi:10.1371/journal.pone.0113052.g003

colony frequency and provided many more iPSC colonies during the second round of iPSC induction (Experiment 2 in Fig. 3a). However, the efficiency of iPSC generation from chimpanzee PMNCs was still lower than that from human blood cells (0.32% vs. 2%, Fig. 3a). We tried picking up the colonies again and expanded them, before shifting the culturing temperature to 38℃ for three days at passage 1 to eliminate the Sendai virus (Fig. 3a). The rate of virus elimination from the chimpanzee iPSCs was similar to that from human iPSCs (65.2% vs. 58.6%).

We then compared the efficiency of iPSC generation with TS12KOS vector to that with the conventional SeV vectors (Experiment 3 in Fig. 3a). Although a high titer (MOI 30) of the conventional SeV vectors could generate chimpanzee iPSCs, TS12KOS vector showed a higher efficiency of iPSC generation (0.073% for the conventional vectors vs. 0.32%, Fig. 3a). Similarly, the elimination rate of SeV was lower than that observed with the conventional vectors, suggesting that our new vector could more efficiently generate the transgene-free iPSCs from chimpanzee blood cells than the conventional SeV vectors.

The chimpanzee iPSC lines exhibited ESC-like morphology and expressed a set of pluripotent markers (Fig. 3d, e), with nested RT-PCR analysis determining that the iPSC lines were negative for SeV genomic material (Fig. 3e). To confirm that these cells were truly derived from chimpanzee, we also performed genomic PCR using chimpanzee-specific primers (Fig. 3f), with different PCR product sizes allowing us to easily distinguish between chimpanzee and human genes and confirming that the chimpanzee-derived samples contained no human DNA fragments [28]. Karyotype analyses showed that the iPSC lines had a normal karyotype, 48XX, further confirming that the iPSC lines were derived from chimpanzee (Fig. 3g).

To investigate the cellular origin of the chimpanzee iPSCs, we performed Southern blot analyses with probes specific for T cell receptor (TCR) DNA (Fig. 3h) [29]. Rearranged bands were detected in all iPSC lines, indicating that they were derived from the chimpanzee T lymphocytes.

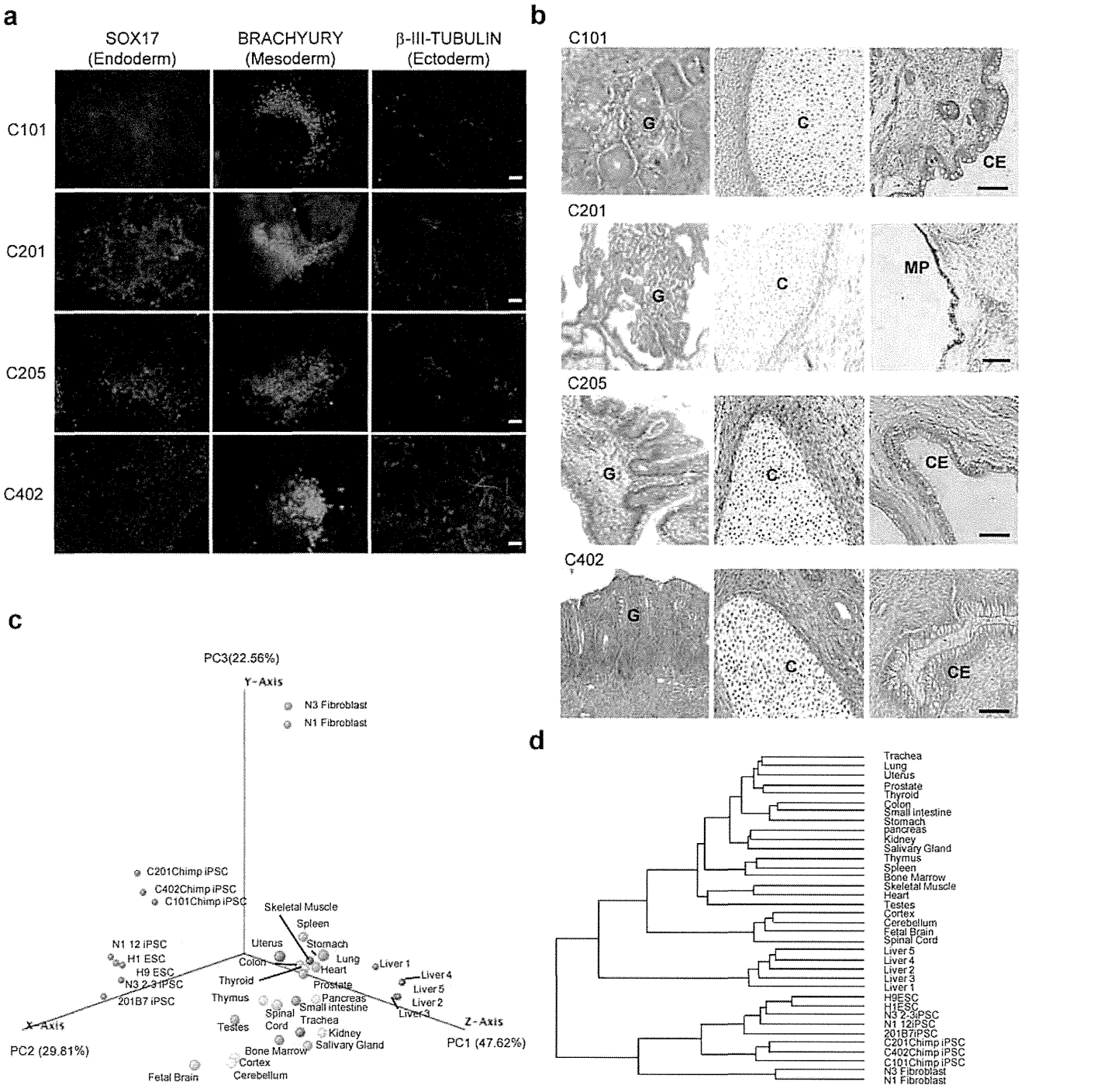

Figure 4. Characterization of chimpanzee iPSCs. (**a**) Differentiation into three germ layers in vitro. The chimpanzee iPSC lines can generate SOX17$^+$ (endoderm), BRACHYURY$^+$ (mesoderm), and βIII-tubulin$^+$ (ectoderm) cells. Scale bars, 100 μm. (**b**) Tissue morphology of a representative teratoma derived from the chimpanzee iPSC lines generated with TS12KOS vector. G, glandular structure (endoderm); C, cartilage (mesoderm); CE, Cuboidal Epithelium structure (ectoderm); MP, melanin pigment (ectoderm). Scale bars, 100 μm. (**c**) Principal Component Analysis. All data sets were classified into three principal components, PC1 (47.62%), PC2 (29.81%), and PC3 (22.56%), and then simplified into three-dimensional scores. Percentage shows the portion of variance in each component. The position of chimpanzee iPSC lines is closely placed to that of human ESCs and iPSCs. (**d**) Hierarchical

clustering of chimpanzee iPSCs, human iPSCs and ESCs. The data sets of all genes investigated were clustered according to Euclidean distance metrics. The data sets of chimpanzee iPSCs, human ESC and iPSC lines, and various human tissues were classified into separate branches. The datasets of human ESCs and various tissues referred for Gene Expression Omnibus datasets, GSE22167 and GSE33846, respectively.

doi:10.1371/journal.pone.0113052.g004

Characterization of chimpanzee iPSC lines

Finally, we investigated the differentiation potential of the chimpanzee iPSCs lines by evaluating in vitro differentiation and teratoma formation (Fig. 4a, b). The appropriate culture conditions induced differentiation into cells representing all three germ layers, ectoderm (βIII-tubulin-positive), mesoderm (BRACHYURY-positive), and endoderm (SOX17-positive) (Fig. 4a). Consistent with this finding, histological analysis revealed that formed teratomas contained descendant markers of all three germ cell layers such as cuboidal epithelia, melanin pigment, cartilage, muscle, and various glandular structures (Fig. 4b). Taken together, the chimpanzee-derived iPSC lines fulfilled the criteria for iPSCs.

We used microarray analysis to further characterize the chimpanzee iPSC lines. The patterns of global gene expression of three chimpanzee iPSC lines were similar to those of human iPSC lines (Fig. 4c). Principal component analysis (PCA) and hierarchical clustering of all genes was conducted to determine overall differences in transcription levels between chimpanzee- and human-derived iPSC lines. Data from human ESCs, iPSCs, fibroblasts, and various tissues were analyzed together with those from chimpanzee iPSCs. Although the chimpanzee iPSC lines were derived from different individuals, their data were grouped by PCA and placed close to those of human ESCs and iPSCs (Fig. 4c). The gene-expression profiles of chimpanzee iPSCs were grouped closely to human ESCs and iPSCs in the same branch, and distinctly separated from the branch containing gene profiles of various human tissues (Fig. 4d). These results suggested that the global gene expression patterns of chimpanzee iPSC lines are generally similar to those of human ESCs and iPSCs.

Discussion

We developed a new temperature-sensitive SeV vector, TS12KOS, and herein demonstrated it to be an efficient tool for generating iPSCs from both human skin fibroblasts and peripheral blood cells. Using this vector, we also generated chimpanzee iPSC lines from peripheral blood cells.

The iPSCs established with our TS12KOS vector could be made virus-free simply by shifting the temperature from 37℃ to 38℃ for 3 days, and transgene-free iPSCs could be generated within a week of isolating the iPSC colonies. Unlike previous techniques that don't use SeV vectors, this system does not require multiple cycles of infection. Furthermore, the efficiency of iPSC generation achieved was 20~100 times higher than that obtained using techniques such as retrovirus, lentivirus, or plasmid vectors [5, 15, 21].

Consideration of the cell source is important when applying iPSC technology to clinical medicine. Although skin fibroblasts are the most common cell type used for generating iPSCs, we consider that peripheral blood cells are preferable because collection is less invasive and is suitable for children and patients with skin or coagulopathy disorders. Here, we demonstrated that the TS12KOS vector generates iPSCs from both skin fibroblasts (~4%) and peripheral blood cells (~2%) with high efficiency.

Overexpression of the four 'reprogramming' factors needed to generate iPSCs was initially mediated by lentivirus and retrovirus vectors in human skin-derived fibroblasts [5, 15]. Although these gene expression systems are stable, they have two potential problems in that the genes encoding the four factors are integrated into the host genome and remain in the resultant iPSCs, and there is a risk of insertional mutagenesis, which can facilitate tumorigenesis *in vivo* [30]. The development of efficient and safe reprograming methods based on using Cre/loxP recombination systems, adenovirus vector, piggyback transposons, microRNA, and protein has suffered from a low frequency of iPSC colony generation, a need for repetitive induction, and retention of a short length of foreign DNA in the host genome [16–18, 31, 32]. A recent study showed that episomal plasmid vectors, which rarely integrate into the host genome, can be used to generate iPSCs from blood cells; however, the efficiency was low (~0.1%) and factors such as p53 knock-down and the transient expression of Epstein-Barr virus nuclear antigen (EBNA) were required in addition to the four reprogramming factors [21]. To overcome these remaining iPSC issues, in this study we developed a new type of SeV vector that can easily and efficiently provide transgene-free iPSC lines from human and chimpanzee blood cells. SeV vectors are minus-strand RNA viruses that express a gene of interest without integration into the host genome [33]. Thus, our vector can overcome the obstacles described above.

The iPSCs derived from nonhuman primates are useful tools for regenerative medicine research because of the similarities in anatomy and physiology between those mammalian species and human, and chimpanzee is a particularly useful such model [9, 10]. Chimpanzee and human share much of their genomic DNA sequences, with only ~1.2% difference [34]. To this end, we also generated transgene-free iPSC lines from chimpanzee blood cells using the new SeV vector. The efficiency of iPSC generation from chimpanzee blood was lower than that from human blood. Stimulation methods of T lymphocytes and human-derived reprogramming factors may affect the efficiency. Nevertheless, further studies are necessary to improve the efficiency of iPSC generation from chimpanzee blood. Recently, other group established the chimpanzee iPSC lines from skin-derived fibroblasts with the retrovirus vector [35]. However, it is difficult in collecting many chimpanzee-derived fibroblasts because of breeding limitation for medical use. Our new vector can easily provide the transgene-free iPSCs from the chimpanzee blood cells that is less limited than other tissues.

The chimpanzee iPSC lines established here showed the requisite pluripotency and other features of established iPSCs and thus could provide us with alternative and highly valuable tools. First, they could be used to generate fresh chimpanzee

cells, which are valuable cell models and difficult to derive from the animal itself due to breeding limitations. For example, neural cells derived from chimpanzee iPSCs could permit us to study neural development and function, and thus facilitate discovery and increased understanding of the substantial neurological differences between human and chimpanzee despite the largely identical genomes.

Furthermore, the technology used herein could be applied to generate iPSCs from nonhuman primates other than chimpanzees. SeV can infect the blood cells of rhesus monkeys, Macaca fascicularis and marmosets, suggesting that our new vector could also easily induce cell reprogramming and iPSC generation from their blood cells [36, 37]. These approaches are expected to improve our ability to better understand and interrogate the distinguishing traits of human and potentially open up a new field in studying the development of human capacity during evolution.

Methods

iPSC Generation and maintenance

All experimental procedures of human samples were approved by the ethics committees, " Ethics committee for Epidemiological and General Research at the Faculty of Life Science, Kumamoto University", "Ethics committee for Human genome and Gene analysis Research at the Faculty of Life Sciences, Kumamoto University" and "Ethics committee for clinical research and advanced medical technology, Kumamoto University" (approval numbers 318, 153 and 1018, respectively) and conformed to the human sample use guidelines of the ethics committees. After explaining our study, the volunteers agreed with our study and signed the sheets of written informed consent.

Human skin biopsies and peripheral blood were collected from healthy volunteers following informed consent under protocols approved by the ethics committee assigning authors. For human fibroblast generation, skin samples were minced and cultured in Dulbecco's modified essential medium (DMEM, Life Technologies) supplemented with 10% fetal bovine serum (FBS). The subsequent fibroblast cultures were expanded for iPS cell induction.

The use of the chimpanzees during the experimental period adhered to the Guidelines for Care and Use of Nonhuman Primates (2010) of the Primate Research Institute of Kyoto University. The ethical committee of the Primate Research Institute of Kyoto University approved the protocols of experimental procedures in this study (Permit Number: 2012-134). Blood samples were obtained from two individuals, Puchi (GAIN-ID:0436) and Ai (GAIN-ID:0434), for routine veterinary and microbiological examination under ketamine anesthesia, and all efforts were made to minimize suffering.

To generate iPS cells from peripheral blood cells, mononuclear cells (MNCs) were isolated by Ficoll gradient method. To stimulate T lymphocytes, MNCs were cultured on anti-CD3 antibody-coated dishes in KBM502 medium (KOHJIN BIO) or RPMI-1640 medium (Invitrogen) supplemented with 10% FBS and IL-2

for five days. In some experiments, instead of anti-CD3 antibody (eBioScience), 10 μg/ml Phytohemagglutinin (PHA, SIGMA) or 1 μg/ml Concanavalin A (Con A, SIGMA) were used for the stimulation.

iPSCs were generated from human skin-derived fibroblasts and human- and chimpanzee-stimulated T lymphocytes as described previously [20]. Briefly, 1×10^5 of the MNCs per well of 48-well plate and 5×10^5 cells of the fibroblasts per well of 6-well plate were seeded one day before infection and then were infected with Sendai virus (SeV) vectors at various multiplicity of infection (MOI) including three, ten and thirty. After two-day culturing for blood cells and seven-day culturing for fibroblasts, the cells infected were harvested by trypsin and re-plated at 5×10^4 cells per 60 mm dish on the mitomycin C (MMC)-treated mouse embryonic fibroblast (MEF) feeder cells. Next day, the medium was replaced in human iPS cell medium. The cultures with new Sendai virus infection were incubated at 36℃ for one week. From 18 to 25 days after infection, colonies were picked up and re-cultured again in the iPS cell medium. In some experiments, FGF2 concentration was modified from 5 ng/ml to 30 ng/ml and NaB was added on day 2 in the iPSC induction. To remove Sendai virus, the temperature of culture shifts from 37℃ to 38℃ for three days at passage 1 or 2 of iPSCs.

Human and chimpanzee iPSC lines were maintained on MMC-treated MEF feeder cells in the iPS medium containing DMEM/F12 (SIGMA) supplemented with 20% KNOCKOUT serum replacement (KSR, Invitrogen), 2 mM L-glutamine (Life technologies), 0.1 mM nonessential amino acids (NEAA, SIGMA), 0.1 mM 2-mercaptoethanol (2ME, SIGMA), 0.5% penicillin and streptomycin (Nacalai Tesque, Japan) and 5 ng/ml or 30 ng/ml basic fibroblast growth factor (bFGF, WAKO, Japan).

Chimpanzee rearing

At the Primate Research Institute of Kyoto University, the subject chimpanzees lived in two mixed-sex groups in an outdoor enclosure that connected to several inside rooms. The outdoor enclosure was separated into two compartments: one was a 700-m^2 outdoor compound with 15-m-high climbing frames, a small stream and numerous trees; the other was a 250-m^2 outdoor compound with climbing frames and two small streams. Chimpanzees could freely access the outdoor enclosure and inside room at all times. The chimpanzees were fed seasonal fruits and vegetables, along with monkey pellets three times per day and were provided feeding-enrichment items between meals on a few occasions.

Generation of Sendai virus (SeV) vectors

Generation and production of temperature-sensitive Sendai virus vectors were performed as described previously [22]. The conventional type of SeV vectors carrying Oct3/4, Sox2, Klf4 and c-Myc were also generated as described previously [22]. To generate TS12 vector, three mutations including D433A, R434A and K437A were introduced into the polymerase-related gene *P*. For TS15 vector

generation, three other mutations, Y942H, L1361C, and L1558I, were inserted into polymerase-related genes *L* of TS12. For "three-in-one" vector, human *KLF4*, *OCT3/4* and *SOX2* genes were inserted between *P* and *M* gene-encoding region in order as described in Fig. 1A. Each gene was sandwiched by *E* (End), *I* (Intervening) and *S* (Start) sequences.

Karyotype analysis

G band analyses of chromosome were performed by Nihon Gene Research Laboratories. Inc. (Sendai, Japan), according to the manufacturer's protocol.

DNA and RNA Isolations and PCR

Genomic DNA was extracted from chimpanzee iPSC lines as described previously [38]. Total RNA was purified with Sepasol Super G reagent (Nacalai Tesque, Japan). Total RNA was transcribed to DNA with Superscript III (Invitrogen) and randam primers (Invitrogen). Genomic PCR and RT-PCR was performed with QuickTaq (TOYOBO, Japan) as described previously [24, 38]. Primers used for Oct3/4, Sox2, Klf4 and c-Myc were designed to detect the expressions of endogenous genes, but not of transgenes. To detect SeV genome, nested RT-PCR was performed. The sequences of primers and amplification conditions are listed in Table S1.

Cell staining and Immunocytochemistry

Alkaline phosphatase staining was performed using the Leukocyte Alkaline Phosphatase kit (SIGMA). For immunocytochemistry, cells were fixed with PBS containing 4% paraformaldehyde for 30 min at 4℃. For the molecules localized in nucleus, samples were treated with 0.2% Triton X-100 for 15 min at room temperature (RT). The cells were washed three times with PBS containing 2% FBS and then incubated overnight at 4℃ in PBS containing 2% FBS with primary antibodies. The list of the primary and secondary antibodies is described in Table S2.

Southern blotting

TCR probe was amplified by PCR as described previously using cDNA of human peripheral blood mononuclear cells and labeled with α^{32}P-dCTP by BcaBEST labeling Kit (Takara Bio Co. Ltd). Commercially available membranes–Hybond-N^+ (GE Healthcare) were used and hybridization was performed as described previously [38].

Differentiation into three germ layer cells

Mesoderm-like cell cultures were specified based upon a previously described protocol [39]. For the embryoid body (EB) formation, iPSC clusters were

transferred to low attachment dishes in DMEM/F12 (SIGMA) supplemented with 20% KSR (Invitrogen) and 10 ng/ml BMP4 (R & D). Next day, the formed EBs were transferred to collagen IV-coated tissue culture plates (BD) in the medoserm induction medium containing alpha-MEM supplemented with 10% FBS, 0.1 mM 2ME, 3 ng/ml Activin (R & D) 10 ng/ml BMP4 and 5 ng/ml bFGF (WAKO). On day 4, the cells were harvested and analyzed for BRACHYURY expression. For endoderm-like cell induction, the culture medium of semi-confluent human iPS cells were switched from the iPS medium to the definitive endoderm differentiation medium containing RPMI1640 supplemented with 2% B27 (Life technologies), 100 ng/ml Activin A (R & D) and 1 mM Sodium butyrate (NaB, SIGMA). The NaB concentration is changed in 0.5 mM on day 2. On day4, the cells were stained with anti-SOX17 antibody.

For neural cell induction, the iPSC clusters were plated onto Geltrex plates (Life Technologies). 24 hours later, the culture medium was switched from the iPSC medium to PSC Neural Induction Medium (Life Technologies) containing Neurobasal medium and PSC neural induction supplement [40]. On day 7, the cells were dissociated with TrypLE express (Life Technologies) and re-seeded onto Geltrex-coated plates in NSC expansion medium containing 50% Neurobasal medium, 50% Advanced DMEM/F12, neural induction supplement and 5 μM Rock inhibitor, Y-27632. On day 14, the cells were stained with anti-betaIII tubulin antibody.

Teratoma formation

Human and chimpanzee iPSC lines grown on MEF feeder layers were collected by collagenase IV treatment and injected into the testis of NOD-SCID immunodeficient mice. Palpable tumors were observed about 12–16 weeks after injection. Tumor samples were collected, fixed in 10% formalin, and processed for paraffin-embedding and hematoxylin-eosin staining following standard procedures.

Microarray analysis

Two hundred fifty ng of total RNA from the chimpanzee iPSCs were labeled with biotin and fragmented according to the manufacturer's protocol (3′ IVT Express kit, Affymetrix). Then, samples were hybridized to a GeneChip Human Genome U133 Plus 2.0 (Affymetrix) Arrays were scanned with a GeneChip Scanner 3000(Affymetrix). Data were analyzed using GeneSpring GX 12.5 software (Agilent technologies). Each chip is normalized to the median of the measurements.

Supporting Information

Figure S1. iPS cell generation with SeV vector carrying *L-Myc* and *Glis1*. (**a**) Schematic structure of Sendai virus (SeV) vectors carrying *L-Myc* and *Glis1*. The exogenous *L-Myc* cDNA is inserted between HN and L positions in TS15 vector.

Glis1 cDNA were inserted between HN and L positions in conventional and TS15 SeV vectors, HNL/TS Glis1 and HNL/TS15 Glis1. We also generated other two vectors, +18/TS Glis1 and +18/TS15 Glis1, which carry Glis1 in the downstreams of Leader in conventional and TS15 SeV vectors. (**b**) Efficiency of iPS cell generation with Myc vectors. The efficiency of iPS cell generation is much lower by *L-Myc* SeV vector than by *c-Myc* SeV vector. iPS cell colonies were identified on day 28 of induction by the appearance of alkaline phosphatase-positive (AP+) colonies with ES cell-like colony morphology. Colony number (right picture) were counted and summarized in left graph. MOI: multiplicity of infection. (**c**) Efficiency of iPS cell generation with various Glis1 vectors. iPS cells were generated with the three factors (K, O, S) plus *Glis1* in the presence (left graph) and absence (right graph) of *c-Myc*. Both cases showed that *Glis1* in SeV vectors did not enhance the efficiency of iPS cell generation.
doi:10.1371/journal.pone.0113052.s001 (TIF)

Figure S2. Experimental design of iPSC induction from chimpanzee blood cells. After collecting mononuclear cells (MNCs) from the chimpanzee blood, MNCs were stimulated with anti-CD3 antibody (Exp. 1) or Con A (Exp. 2 and 3) for five days. One day later after the infection of the sendai virus carrying *OCT3/4*, *KLF4*, *SOX2* and *cMYC*, the cells were transferred on the MEFs with 5 ng/ml (Exp. 1) or 30 ng/ml (Exp.2 and 3) FGF2.
doi:10.1371/journal.pone.0113052.s002 (TIF)

Figure S3. Comparing the chimpanzee with human conditions in iPSC generation. Using human blood cells from two volunteers (volunteer 4 and 5), the condition of chimpanzee with 30 ng/ml FGF2 is compared with that of human with 5 ng/ml in iPSC generation. The efficiency of iPSC generation with 30 ng/ml FGF is slightly but not significantly lower than that with 5 ng/ml FGF2.
doi:10.1371/journal.pone.0113052.s003 (TIF)

Table S1. Sequences and PCR conditions of primers sets for PCR.
doi:10.1371/journal.pone.0113052.s004 (DOCX)

Table S2. List of antibodies and their conditions for staining.
doi:10.1371/journal.pone.0113052.s005 ((DOCX))

Author Contributions

Conceived and designed the experiments: TE. Performed the experiments: YF TK M. Hamasaki YS MS NF. Analyzed the data: YF TK M. Hamasaki YS MS NF. Contributed reagents/materials/analysis tools: NF HB M. Hasegawa SY SK SS TM HA. Wrote the paper: TE.

References

1. **Takahashi K, Yamanaka S** (2006) Induction of pluripotent stem cells from mouse embryonic and adult fibroblast cultures by defined factors. Cell 126: 663–676.

2. **Liao J, Cui C, Chen S, Ren J, Chen J, et al.** (2009) Generation of induced pluripotent stem cell lines from adult rat cells. Cell Stem Cell 4: 11–15.

3. **Tomioka I, Maeda T, Shimada H, Kawai K, Okada Y, et al.** (2010) Generating induced pluripotent stem cells from common marmoset (Callithrix jacchus) fetal liver cells using defined factors, including Lin28. Genes Cells 15: 959–969.

4. **Liu H, Zhu F, Yong J, Zhang P, Hou P, et al.** (2008) Generation of induced pluripotent stem cells from adult rhesus monkey fibroblasts. Cell Stem Cell 3: 587–590.

5. **Takahashi K, Tanabe K, Ohnuki M, Narita M, Ichisaka T, et al.** (2007) Induction of pluripotent stem cells from adult human fibroblasts by defined factors. Cell 131: 861–872.

6. **Wu Z, Chen J, Ren J, Bao L, Liao J, et al.** (2009) Generation of pig induced pluripotent stem cells with a drug-inducible system. J Mol Cell Biol 1: 46–54.

7. **Wu Y, Zhang Y, Mishra A, Tardif SD, Hornsby PJ** (2010) Generation of induced pluripotent stem cells from newborn marmoset skin fibroblasts. Stem Cell Res 4: 180–188.

8. **Hankowski KE, Hamazaki T, Umezawa A, Terada N** (2011) Induced pluripotent stem cells as a next-generation biomedical interface. Lab Invest 91: 972–977.

9. **Hackett TA, Preuss TM, Kaas JH** (2001) Architectonic identification of the core region in auditory cortex of macaques, chimpanzees, and humans. J Comp Neurol 441: 197–222.

10. **Rogers J, Gibbs RA** (2014) Comparative primate genomics: emerging patterns of genome content and dynamics. Nat Rev Genet 15: 347–359.

11. **Mubiru JN, Yang AS, Olsen C, Nayak S, Livi CB, et al.** (2014) Analysis of prostate-specific antigen transcripts in chimpanzees, cynomolgus monkeys, baboons, and African green monkeys. PLoS One 9: e94522.

12. **Rearden A** (1986) Evolution of glycophorin A in the hominoid primates studied with monoclonal antibodies, and description of a sialoglycoprotein analogous to human glycophorin B in chimpanzee. J Immunol 136: 2504–2509.

13. **Gonzalez JP, Prugnolle F, Leroy E** (2013) Men, primates, and germs: an ongoing affair. Curr Top Microbiol Immunol 365: 337–353.

14. **Wernig M, Meissner A, Foreman R, Brambrink T, Ku M, et al.** (2007) In vitro reprogramming of fibroblasts into a pluripotent ES-cell-like state. Nature 448: 318–324.

15. **Sommer CA, Stadtfeld M, Murphy GJ, Hochedlinger K, Kotton DN, et al.** (2009) Induced pluripotent stem cell generation using a single lentiviral stem cell cassette. Stem Cells 27: 543–549.

16. **Woltjen K, Michael IP, Mohseni P, Desai R, Mileikovsky M, et al.** (2009) piggyBac transposition reprograms fibroblasts to induced pluripotent stem cells. Nature 458: 766–770.

17. **Zhou H, Wu S, Joo JY, Zhu S, Han DW, et al.** (2009) Generation of induced pluripotent stem cells using recombinant proteins. Cell Stem Cell 4: 381–384.

18. **Miyoshi N, Ishii H, Nagano H, Haraguchi N, Dewi DL, et al.** (2011) Reprogramming of mouse and human cells to pluripotency using mature microRNAs. Cell Stem Cell 8: 633–638.

19. **Okita K, Nakagawa M, Hyenjong H, Ichisaka T, Yamanaka S** (2008) Generation of mouse induced pluripotent stem cells without viral vectors. Science 322: 949–953.

20. **Seki T, Yuasa S, Oda M, Egashira T, Yae K, et al.** (2010) Generation of induced pluripotent stem cells from human terminally differentiated circulating T cells. Cell Stem Cell 7: 11–14.

21. **Okita K, Yamakawa T, Matsumura Y, Sato Y, Amano N, et al.** (2013) An efficient nonviral method to generate integration-free human-induced pluripotent stem cells from cord blood and peripheral blood cells. Stem Cells 31: 458–466.

22. **Fusaki N, Ban H, Nishiyama A, Saeki K, Hasegawa M** (2009) Efficient induction of transgene-free human pluripotent stem cells using a vector based on Sendai virus, an RNA virus that does not integrate into the host genome. Proc Jpn Acad Ser B Phys Biol Sci 85: 348–362.

23. **Ban H, Nishishita N, Fusaki N, Tabata T, Saeki K, et al.** (2011) Efficient generation of transgene-free human induced pluripotent stem cells (iPSCs) by temperature-sensitive Sendai virus vectors. Proc Natl Acad Sci U S A 108: 14234–14239.

24. **Hamasaki M, Hashizume Y, Yamada Y, Katayama T, Hohjoh H, et al.** (2012) Pathogenic mutation of ALK2 inhibits induced pluripotent stem cell reprogramming and maintenance: mechanisms of reprogramming and strategy for drug identification. Stem Cells 30: 2437–2449.

25. **Nakagawa M, Takizawa N, Narita M, Ichisaka T, Yamanaka S** (2010) Promotion of direct reprogramming by transformation-deficient Myc. Proc Natl Acad Sci U S A 107: 14152–14157.

26. **Maekawa M, Yamaguchi K, Nakamura T, Shibukawa R, Kodanaka I, et al.** (2011) Direct reprogramming of somatic cells is promoted by maternal transcription factor Glis1. Nature 474: 225–229.

27. **Mali P, Chou BK, Yen J, Ye Z, Zou J, et al.** (2010) Butyrate greatly enhances derivation of human induced pluripotent stem cells by promoting epigenetic remodeling and the expression of pluripotency-associated genes. Stem Cells 28: 713–720.

28. **McLean CY, Reno PL, Pollen AA, Bassan AI, Capellini TD, et al.** (2011) Human-specific loss of regulatory DNA and the evolution of human-specific traits. Nature 471: 216–219.

29. **Langerak AW, Wolvers-Tettero IL, van Dongen JJ** (1999) Detection of T cell receptor beta (TCRB) gene rearrangement patterns in T cell malignancies by Southern blot analysis. Leukemia 13: 965–974.

30. **Nakagawa M, Koyanagi M, Tanabe K, Takahashi K, Ichisaka T, et al.** (2008) Generation of induced pluripotent stem cells without Myc from mouse and human fibroblasts. Nat Biotechnol 26: 101–106.

31. **Stadtfeld M, Nagaya M, Utikal J, Weir G, Hochedlinger K** (2008) Induced pluripotent stem cells generated without viral integration. Science 322: 945–949.

32. **Soldner F, Hockemeyer D, Beard C, Gao Q, Bell GW, et al.** (2009) Parkinson's disease patient-derived induced pluripotent stem cells free of viral reprogramming factors. Cell 136: 964–977.

33. **Nagai Y TA, Irie T, Yonemitsu Y, Gotoh B** (2011) Sendai virus: Evolution from mouse pathogen to a state-of-the-art tool in virus research and biotechnology. The biology of Paramyxoviruses Samal SK, Ed, Caister Academic Press, Norfolk, UK: 115–173.

34. **Kehrer-Sawatzki H, Cooper DN** (2007) Understanding the recent evolution of the human genome: insights from human-chimpanzee genome comparisons. Hum Mutat 28: 99–130.

35. **Marchetto MC, Narvaiza I, Denli AM, Benner C, Lazzarini TA, et al.** (2013) Differential L1 regulation in pluripotent stem cells of humans and apes. Nature 503: 525–529.

36. **Sasaki K, Inoue M, Shibata H, Ueda Y, Muramatsu SI, et al.** (2005) Efficient and stable Sendai virus-mediated gene transfer into primate embryonic stem cells with pluripotency preserved. Gene Ther 12: 203–210.

37. **Fusaki N BH, Nagai Y** (2014) Induction of Human Pluripotent Stem Cells by the Sendai Virus Vector: Establishment of a Highly Efficient and Footprint-Free System. Sendai Virus Vector: Advantages and Applications Springer 171–183.

38. **Kitagawa M, Takebe A, Ono Y, Imai T, Nakao K, et al.** (2012) Phf14, a novel regulator of mesenchyme growth via platelet-derived growth factor (PDGF) receptor-alpha. J Biol Chem 287: 27983–27996.

39. **Sakurai H, Era T, Jakt LM, Okada M, Nakai S, et al.** (2006) In vitro modeling of paraxial and lateral mesoderm differentiation reveals early reversibility. Stem Cells 24: 575–586.

40. **Yan Y, Shin S, Jha BS, Liu Q, Sheng J, et al.** (2013) Efficient and rapid derivation of primitive neural stem cells and generation of brain subtype neurons from human pluripotent stem cells. Stem Cells Transl Med 2: 862–870.

Biochemical and Biophysical Research Communications 450 (2014) 942–947

Contents lists available at ScienceDirect

Biochemical and Biophysical Research Communications

journal homepage: www.elsevier.com/locate/ybbrc

Identification of SIV Nef CD8$^+$ T cell epitopes restricted by a MHC class I haplotype associated with lower viral loads in a macaque AIDS model

Takushi Nomura [a,*], Hiroyuki Yamamoto [a], Naofumi Takahashi [a], Taeko K. Naruse [b], Akinori Kimura [b], Tetsuro Matano [a,c,*]

[a] AIDS Research Center, National Institute of Infectious Diseases, 1-23-1 Toyama, Shinjuku-ku, Tokyo 162-8640, Japan
[b] Department of Molecular Pathogenesis, Medical Research Institute, Tokyo Medical and Dental University, 2-3-10 Kandasurugadai, Chiyoda-ku, Tokyo 101-0062, Japan
[c] The Institute of Medical Science, The University of Tokyo, 4-6-1 Shirokanedai, Minato-ku, Tokyo 108-8639, Japan

ARTICLE INFO

Article history:
Received 6 June 2014
Available online 24 June 2014

Keywords:
HIV
SIV
CD8$^+$ T cell
MHC-I
Epitope

ABSTRACT

Virus-specific CD8$^+$ T-cell responses are crucial for the control of human immunodeficiency virus (HIV) and simian immunodeficiency virus (SIV) replication. Multiple studies on HIV-infected individuals and SIV-infected macaques have indicated association of several major histocompatibility complex class I (MHC-I) genotypes with lower viral loads and delayed AIDS progression. Understanding of the viral control mechanism associated with these MHC-I genotypes would contribute to the development of intervention strategy for HIV control. We have previously reported a rhesus MHC-I haplotype, *90-120-Ia*, associated with lower viral loads after SIVmac239 infection. $Gag_{206-216}$ and $Gag_{241-249}$ epitope-specific CD8$^+$ T-cell responses have been shown to play a central role in the reduction of viral loads, whereas the effect of Nef-specific CD8$^+$ T-cell responses induced in all the *90-120-Ia*$^+$ macaques on SIV replication remains unknown. Here, we identified three CD8$^+$ T-cell epitopes, Nef_{9-19}, Nef_{89-97}, and $Nef_{193-203}$, associated with *90-120-Ia*. Nef_{9-19} and $Nef_{193-203}$ epitope-specific CD8$^+$ T-cell responses frequently selected for mutations resulting in viral escape from recognition by these CD8$^+$ T cells, indicating that these CD8$^+$ T cells exert strong suppressive pressure on SIV replication. Results would be useful for elucidation of the viral control mechanism associated with *90-120-Ia*.

1. Introduction

In human immunodeficiency virus (HIV) and simian immunodeficiency virus (SIV) infections, host immune responses fail to eradicate viruses and allow persistent infection, leading to AIDS progression. Unlike most acute virus infections, effective neutralizing antibody responses are not efficiently induced in early HIV/SIV infection [1]. Virus-specific CD8$^+$ T-cell responses play an important role in the control of HIV/SIV replication [2–6]. CD8$^+$ T cells recognize antigenic peptides bound to polymorphic major histocompatibility complex class I (MHC-I) molecules, whose genotypes affect CD8$^+$ T-cell responses [7,8]. Several MHC-I genotypes have been shown to be associated with lower viral loads and slower disease progression in HIV/SIV infections [9–14]. Understanding of the viral control mechanism associated with these protective MHC-I alleles would contribute to the development of intervention strategy for HIV control.

Recent vaccine trials in macaque AIDS models have shown a possibility of SIV control by effective CD8$^+$ T-cell responses [15–19]. It has been indicated that CD8$^+$ T cells targeting Gag are effective against HIV/SIV infection [20–23]. Furthermore, current studies have suggested that Nef- and Vif-specific CD8$^+$ T-cell responses can contribute to SIV control in macaque AIDS models [24,25].

We have previously reported a rhesus MHC-I haplotype, *90-120-Ia*, associated with lower viral loads after SIVmac239 challenge [14]. In that study, those Burmese rhesus macaques possessing *90-120-Ia* had lower set-point plasma viral loads (geometric mean at 1 year after SIV challenge: 1.5×10^4 copies/ml); two of them controlled viremia for more than 4 years while the remaining four developed AIDS in 4 years. Our vaccine trial has shown that all the *90-120-Ia*$^+$ macaques immunized with DNA-prime/Gag-expressing Sendai virus (SeV-Gag) vector-boost controlled a SIVmac239 challenge [26]. Mamu-A1*043:01-restricted $Gag_{206-216}$ (IINEEAADWDL) and Mamu-A1*065:01-restricted $Gag_{241-249}$ (SSVDEQIQW) epitope-specific CD8$^+$ T-cell responses were responsible for this viral control

* Corresponding authors. Address: AIDS Research Center, National Institute of Infectious Diseases, 1-23-1 Toyama, Shinjuku-ku, Tokyo 162-8640, Japan. Fax: +81 3 5285 1165.
E-mail addresses: nomutaku@nih.go.jp (T. Nomura), tmatano@nih.go.jp (T. Matano).

http://dx.doi.org/10.1016/j.bbrc.2014.06.072
0006-291X/

[26–28]. SIVmac239-infected *90-120-Ia*$^+$ macaques also elicited CD8$^+$ T-cell responses targeting Nef, which may be involved in viral control [14]. In the present study, we determined Nef CD8$^+$ T-cell epitopes associated with this MHC-I haplotype *90-120-Ia*.

2. Materials and methods

2.1. Samples

The present study used frozen plasma and peripheral mononuclear cell (PBMC) samples derived from ten Burmese rhesus macaques (*Macaca mulatta*) possessing MHC-I haplotype *90-120-Ia*. Our previous SIVmac239 challenge experiments using these animals [14,26–28] have been carried out in Tsukuba Primate Research Center in National Institute of Biomedical Innovation (NIBP) with the help of the Corporation for Production and Research of Laboratory Primates. These studies were approved by the Committee on the Ethics of Animal Experiments of NIBP under the guideline for animal experiments at NIBP and the National Institute of Infectious Diseases which is in accordance with the Guidelines for Proper Conduct of Animal Experiments established by the Science Council of Japan (http://www.scj.go.jp/ja/info/kohyo/pdf/kohyo-20-k16-2e.pdf).

Macaques R06-037, R07-004, and R07-009 were unvaccinated and intravenously challenged with SIVmac239 [14]. Macaques R03-018 and R07-007 received a DNA-prime/SeV-boost vaccine eliciting $Gag_{206-216}$- and $Gag_{241-249}$-specific CD8$^+$ T-cell responses, respectively, before SIVmac239 challenge as described before [27,28]. Macaques R06-035, R06-041, R05-004, R05-027, and R07-005 received a DNA-prime/SeV-Gag-boost as described before [26]. Macaques R06-035 and R06-041 were intravenously challenged with SIVmac239Gag216S244E, a SIVmac239 carrying two *gag* mutations, GagL216S and GagD244E, leading to a leucine (L)-to-serine (S) substitution at the 216th amino acid (aa) and an aspartic acid (D)-to-glutamic acid (E) substitution at the 244th aa in Gag, whereas macaques R05-004, R05-027, and R07-005 with SIVmac239Gag216S244E247L312V373T, a SIVmac239 carrying five *gag* mutations, GagL216S, GagD244E, GagI247L (isoleucine [I] to L at the 247th aa), GagA312V (alanine [A] to valine [V] at the 312th aa), and GagA373T (A to threonine [T] at the 373rd aa) [26].

The determination of macaque MHC-I haplotypes was based on the family study in combination with the reference strand-mediated conformation analysis of *Mamu-A* and *Mamu-B* genes and detection of major *Mamu-A* and *Mamu-B* alleles by cloning the reverse transcription (RT)-PCR products [14,29,30]. Confirmed MHC-I alleles consisting of the MHC-I haplotype *90-120-Ia* are *Mamu-A1*043:01* (GenBank accession number AB444869), *Mamu-A1*065:01* (AB444921), *Mamu-B*061:03* (AB430442), *Mamu-B*068:04* (AM902571), and *Mamu-B*089:01* (EF580172).

2.2. Sequencing analysis of plasma viral genomes

Viral RNAs were extracted using the High Pure Viral RNA kit (Roche Diagnostics) from plasma. Fragments of cDNAs encoding SIVmac239 Nef were amplified by nested RT-PCR from plasma RNAs and subjected to direct sequencing by using dye terminator chemistry and an automated DNA sequencer (Applied Biosystems) [33].

2.3. Analysis of SIV peptide-specific CD8$^+$ T-cell responses

SIV peptide-specific CD8$^+$ T-cell responses were measured by flow-cytometric analysis of interferon-γ (IFN-γ) induction [25]. PBMCs (2.5×10^6 cells) were cocultured for 6 h with autologous herpesvirus papio-immortalized B-lymphoblastoid cell lines (B-LCLs; 1.0×10^6 cells) pulsed with 1–5 μM or indicated concentrations of peptides designed for epitope mapping in 96-well V-bottom microwell plates. Intracellular IFN-γ staining was performed using a Cytofix Cytoperm kit (BD). Fluorescein isothiocyanate-conjugated anti-human CD4 (BD), peridinin chlorophyll protein (PerCP)-conjugated anti-human CD8 (BD), allophycocyanin Cy7 (APC-Cy7)-conjugated anti-human CD3 (BD), and phycoerythrin (PE)-conjugated anti-human IFN-γ antibodies (Biolegend) were used. Specific T-cell frequencies were calculated by subtracting nonspecific IFN-γ$^+$ T-cell frequencies from those after peptide-specific stimulation. Specific T-cell frequencies less than 100 cells per million PBMCs were considered negative.

3. Results and discussion

3.1. Identification of three Nef CD8$^+$ T-cell epitopes associated with MHC-I haplotype 90–120-Ia

In our previous study [14], we examined viral genome sequences 1 year after SIVmac239 challenge in four groups of Burmese rhesus macaques possessing MHC-I haplotypes *90-120-Ia*, *90-120-Ib*, *90-010-Ie*, and *90-088-Ij*, respectively. Then, in the present study, we compared *nef* sequences in the four macaques possessing *90-120-Ia* with those in the remaining three groups ($n = 14$). Amino acid sequences revealed three regions in Nef, Nef12 (the 12th aa), Nef89/90 (the 89th or 90th aa), and Nef201/202 (the 201st or 202nd aa), which had substitutions in all *90-120-Ia*$^+$ animals but mostly not in others. Indeed, substitutions at Nef12 were observed only in two of the fourteen *90-120-Ia*-negative animals while substitutions at Nef89/90 or Nef201/202 were detected in none of them.

We tried to map CD8$^+$ T-cell epitopes around the regions described above to examine whether these *90-120-Ia*-associated *nef* mutations resulting in the Nef12, Nef89/90, and Nef201/202 amino acid substitutions were selected by CD8$^+$ T cells. Analysis using available samples derived from ten *90-120-Ia*$^+$ macaques identified three CD8$^+$ T-cell epitopes, Nef_{9-19} (RSRPSGDLRQR), Nef_{89-97} (DIDEEDDDL), and $Nef_{193-203}$ (YLMHPAQTSQW) (Fig. 1A). The endpoint peptide concentrations for CD8$^+$ T-cell responses were 10–100 nM against Nef_{9-19} epitope and 1–10 nM against $Nef_{193-203}$ (Fig. 1B). The endpoint was very low, less than 0.1 nM, for Nef_{89-97} epitope (Fig. 1B), indicating extremely high binding affinity of this epitope.

3.2. Determination of MHC-I alleles restricting CD8$^+$ T-cell epitopes

Nef_{9-19} epitope-specific CD8$^+$ T-cell responses in the early phase of SIV infection were examined in six *90-120-Ia*$^+$ animals, all of which showed positive responses (Fig. 2A), indicating that this epitope is associated with MHC-I haplotype *90-120-Ia*. On the other hand, Nef_{89-97} and $Nef_{193-203}$ epitope-specific CD8$^+$ T-cell responses in the early phase were detected not in all but in three of the seven and two of the four examined *90-120-Ia*$^+$ animals, respectively (Fig. 2A).

We then tried to determine *90-120-Ia*-derived MHC-I alleles restricting these CD8$^+$ T-cell epitopes. HLA-A/B/C-negative human 721.221 cell lines expressing *Mamu-A1*043:01*, *Mamu-A1*065:01*, and *Mamu-B*061:03* were available for the analysis. Nef_{89-97}-specific CD8$^+$ T-cell responses were detected on *Mamu-A1*043:01*-expressing 721.221 cells, whereas $Nef_{193-203}$-specific CD8$^+$ T-cell responses were detected on *Mamu-A1*065:01*-expressing 721.221 cells (Fig. 2B). These results indicate that the Nef_{89-97} and $Nef_{193-203}$ epitopes are restricted by Mamu-A1*043:01 and Mamu-A1*065:01, respectively. However, Nef_{9-19} epitope-specific CD8$^+$ T-cell responses were not detected on any of 721.221 cells expressing *Mamu-A1*043:01*, *Mamu-A1*065:01*, or *Mamu-B*061:03*,

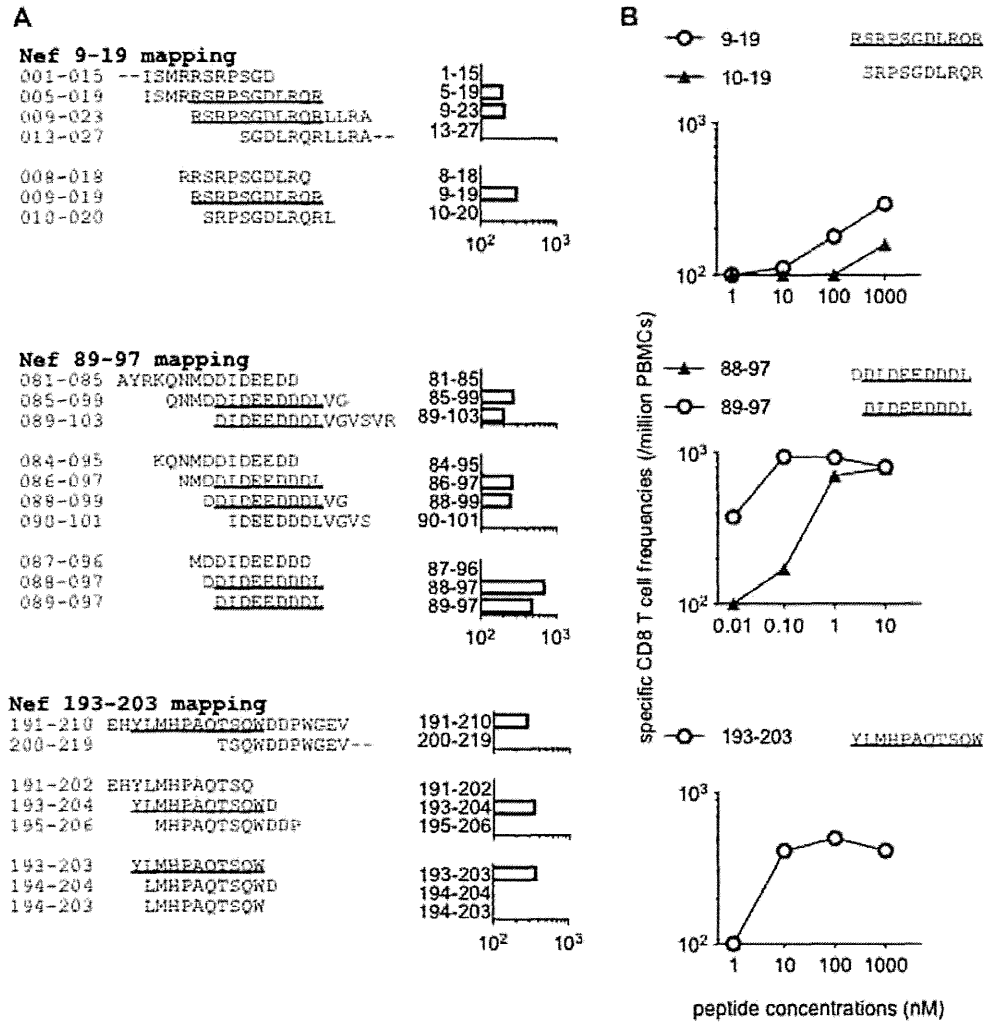

Fig. 1. Mapping of CD8$^+$ T-cell epitopes, Nef_{9-19}, Nef_{89-97}, and $Nef_{193-203}$. (A) Summarized data for mapping of Nef_{9-19} (top panels), Nef_{89-97} (middle), and $Nef_{193-203}$ (bottom) epitopes using PBMCs of SIV-infected *90-120-Ia*$^+$ animals. CD8$^+$ T-cell frequencies specific for the indicated peptides are shown (/million PBMCs). Representative results using PBMCs from R05-027 and R06-041 (top), R03-018 (middle), and R07-004 and R07-007 (bottom) are shown. (B) CD8$^+$ T-cell responses under the indicated concentrations of Nef_{9-19} and Nef_{10-19} (top panel), Nef_{88-97} and Nef_{89-97} (middle), and $Nef_{193-203}$ (bottom) peptides. Representative results using PBMCs from R05-004 (top), R03-018 (middle), and R07-009 (bottom) are shown.

implying that this epitope is restricted by a *90-120-Ia*-derived MHC-I molecule other than the above three (Fig. 2B).

3.3. Mutations resulting in viral escape from CD8$^+$ T-cell recognition

In our previous study [14], SIV-infected *90-120-Ia*$^+$ macaques had mutations resulting in Nef12, Nef89/90, and Nef201/202 amino acid substitutions as described above. The substituted amino acids were different at Nef89/90 in individual four animals, but three of the four had the same substitutions at Nef12 and Nef201, NefP12Q (proline [P]-to-glutamine [Q]) and NefS201Y (S-to-tyrosine [Y]), respectively. We examined whether these two *90-120-Ia*-associated *nef* mutations result in viral escape from CD8$^+$ T-cell responses specific for the epitopes we identified. Nef_{9-19} peptide-specific CD8$^+$ T-cell responses were reduced by the NefP12Q substitution (Fig. 3A). Also, the NefP12T substitution (a P-to-T substitution at the 12th aa in Nef) that was observed in the remaining one SIV-infected *90-120-Ia*$^+$ macaque resulted in viral escape from Nef_{9-19}-specific CD8$^+$ T-cell responses. $Nef_{193-203}$ peptide-specific CD8$^+$ T-cell responses were reduced by the NefS201Y (Fig. 3A). Selection of these escape mutations in SIV infection implies that these Nef_{9-19} and $Nef_{193-203}$ epitope-specific CD8$^+$ T cells exert suppressive pressure on SIV replication. The latter $Nef_{193-203}$ epitope overlaps with previously-reported MW9 ($Nef_{195-203}$) and HW8 ($Nef_{196-203}$) epitopes [32,33]. The MW9 is restricted by Mamu-B*17 [12], a protective MHC-I against SIVmac239 infection, while the HW8 is restricted by a MHC-I in a group of Mauritian cynomolgus macaques that frequently control SIVmac239 replication. Thus, this $Nef_{193-203}$ region may be a promising CD8$^+$ T-cell target for SIV control.

Further analysis of viral *nef* nucleotide sequences found relatively rapid selection of a mutation encoding Nef12, NefP12Q, NefP12S, or NefS13P, in two months after SIV infection in macaques R05-004, R05-027, R06-035, R06-041, and R07-005 (Fig. 3B). The NefP12S and NefS13P substitutions also resulted in viral escape from Nef_{9-19}-specific CD8$^+$ T-cell responses (Fig. 3A). However, no mutation was selected in the region encoding Nef_{89-97} or $Nef_{193-203}$ epitope in two months (Fig. 3B). In the early phase, Nef_{9-19}-specific CD8$^+$ T-cell responses were induced in all whereas Nef_{89-97}- and $Nef_{193-203}$-specific CD8$^+$ T-cell responses were detectable only in some of them, as described above. These results suggest that *90-120-Ia*$^+$ macaques predominantly elicit Nef_{9-19}-specific CD8$^+$ T-cell responses resulting in selection of Nef12/13 mutations in the early phase of SIV infection, followed by induction of Nef_{89-97}- and $Nef_{193-203}$-specific CD8$^+$ T-cell responses resulting in selection of Nef89/90 and Nef201/202 mutations in the chronic phase.

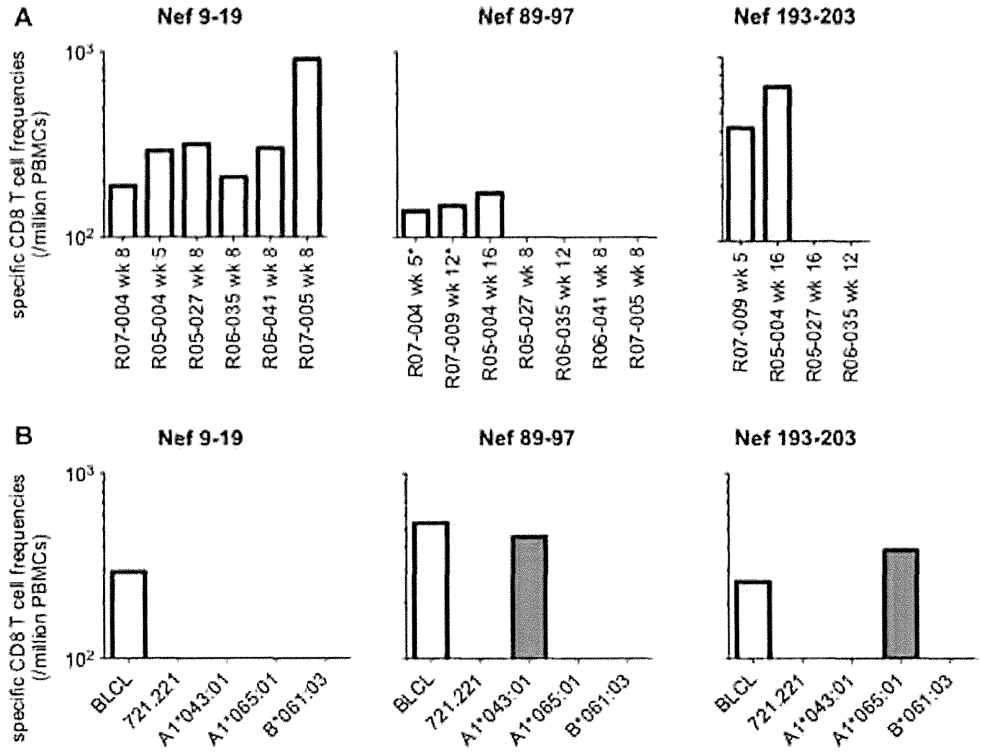

Fig. 2. Nef_{9-19}, Nef_{89-97}, and $Nef_{193-203}$ epitope-specific $CD8^+$ T-cell responses. (A) $CD8^+$ T-cell responses specific for Nef_{9-19} (left panel), Nef_{89-97} (middle), and $Nef_{193-203}$ (right) epitopes in the early phase of SIV infection in *90-120-Ia*$^+$ macaques. The asterisk indicates $CD8^+$ T-cell responses specific for Nef_{86-97} peptide. (B) Nef_{9-19}- (left panel), Nef_{89-97}- (middle), and $Nef_{193-203}$-specific (right) $CD8^+$ T-cell responses after coculture with peptide-pulsed B-LCLs, 721.221 cells, or 721.221 cells expressing *Mamu-A1*043:01*, *Mamu-A1*065:01*, or *Mamu-B*061:03*. These cells were pulsed with 1,000 nM Nef_{9-19} peptides (left), 1 nM Nef_{89-97} peptides (middle), and 100 nM $Nef_{193-203}$ peptides (right), respectively. Representative results using PBMCs from R06-035 for Nef_{9-19}, R03-018 for Nef_{89-97}, and R07-004 for $Nef_{193-203}$ are shown.

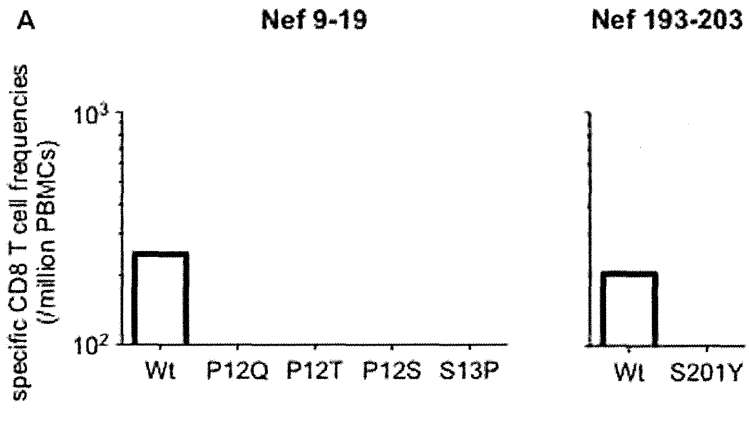

B

Nef	9-19	89-97	193-203
	RSRPSGDLRQR	DIDEEDDDL	YLMHPAQTSQW
R05-004	---S-------	---------	----------
R05-027	---Q-------	---------	----------
R06-035	---SP------	---------	----------
R06-041	---S-------	---------	----------
R07-005	----P------	---------	----------G

Fig. 3. $CD8^+$ T-cell escape mutations. (A) $CD8^+$ T-cell responses specific for the wild-type or mutant Nef_{9-19} peptides with the indicated substitutions (left panel) or the wild-type or a mutant $Nef_{193-203}$ peptide with S201Y substitution (right). Representative results using PBMCs from R07-005 for Nef_{9-19} and R07-004 for $Nef_{193-203}$ are shown. (B) Predominant nonsynonymous mutations in plasma viral *nef* regions encoding Nef_{9-19}, Nef_{89-97}, and $Nef_{193-203}$ epitopes in 3 months after SIV challenge in *90-120-Ia*$^+$ macaques. Amino acid substitutions are shown.

Our previous study [14] frequently found $CD8^+$ T-cell responses targeting Vif and a viral genome mutation resulting in VifP115S substitution (a P-to-S substitution at the 115th aa in Vif) in SIV-infected *90-120-Ia*$^+$ macaques. Then, in the present study, we identified a $CD8^+$ T-cell epitope, $Vif_{114-124}$ (FPCFTAGEVRR). The endpoint peptide concentration for $Vif_{114-124}$-specific $CD8^+$ T-cell

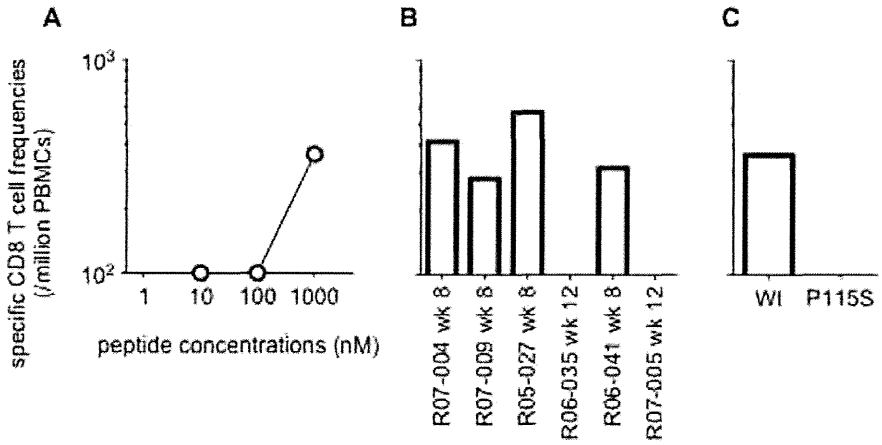

Fig. 4. Characterization of $Vif_{114-124}$ epitope-specific $CD8^+$ T-cell responses. (A) $CD8^+$ T-cell responses under the indicated concentrations of $Vif_{114-124}$ peptides. A representative result using PBMCs from R07-004 is shown. (B) $Vif_{114-124}$-specific $CD8^+$ T-cell responses in the early phase of SIV infection in *90-120-Ia*$^+$ macaques. (C) $CD8^+$ T-cell responses specific for the wild-type or a mutant $Vif_{114-124}$ peptide with P115S substitution. A representative result using PBMCs from R07-004 is shown.

responses was very high, more than 100 nM, indicating lower binding affinity of this epitope (Fig. 4A). $Vif_{114-124}$ epitope-specific $CD8^+$ T-cell responses were detected in the early phase in four of the six examined *90-120-Ia*$^+$ animals (Fig. 4B). The VifP115S substitution resulted in diminishment of $Vif_{114-124}$ peptide-specific $CD8^+$ T-cell responses, suggesting selective pressure by $CD8^+$ T cells targeting this epitope (Fig. 4C).

In summary, we identified three *90-120-Ia*-associated Nef $CD8^+$ T-cell epitopes, Nef_{9-19}, Nef_{89-97}, and $Nef_{193-203}$, in addition to the three previously-identified Gag epitopes, $Gag_{206-216}$, $Gag_{241-249}$, and $Gag_{373-380}$ [31]. Additionally, we identified a Vif $CD8^+$ T-cell epitope, $Vif_{114-124}$. In our previous study [26], all the *90-120-Ia*$^+$ macaques vaccinated with DNA-prime/SeV-Gag-boost controlled SIVmac239 replication without detectable viral loads after week 5 post-challenge, whereas those vaccinated animals (R05-004, R05-027, R06-035, R06-041, and R07-005) failed to show such rapid control of a challenge with SIVs carrying $Gag_{206-216}$-, $Gag_{241-249}$-, and $Gag_{373-380}$-specific $CD8^+$ T-cell escape mutations. This indicates that these $Gag_{206-216}$, $Gag_{241-249}$, and $Gag_{373-380}$ epitope-specific $CD8^+$ T-cell responses are responsible for the rapid SIVmac239 control. Macaques R05-004 and R05-027 showed persistent viremia and developed AIDS, whereas the remaining three (R06-035, R06-041, and R07-005) exhibited lower viral loads. The present study suggests involvement of Nef epitope-specific $CD8^+$ T-cell responses in this suppression of SIV replication in *90-120-Ia*$^+$ macaques.

Acknowledgments

This work was supported by a Grant-in-Aid for Scientific Research on Innovative Areas (#25115520) from the Ministry of Education, Culture, Sports, Science, and Technology in Japan and grants-in-aid from the Ministry of Health, Labor, and Welfare in Japan.

References

[1] D.R. Burton, R.C. Desrosiers, R.W. Doms, W.C. Koff, P.D. Kwong, J.P. Moore, G.J. Nabel, J. Sodroski, I.A. Wilson, R.T. Wyatt, HIV vaccine design and the neutralizing antibody problem, Nat. Immunol. 5 (2004) 233–236.
[2] R.A. Koup, J.T. Safrit, Y. Cao, C.A. Andrews, G. McLeod, W. Borkowsky, C. Farthing, D.D. Ho, Temporal association of cellular immune responses with the initial control of viremia in primary human immunodeficiency virus type 1 syndrome, J. Virol. 68 (1994) 4650–4655.
[3] P. Borrow, H. Lewicki, B.H. Hahn, G.M. Shaw, M.B. Oldstone, Virus-specific $CD8^+$ cytotoxic T-lymphocyte activity associated with control of viremia in primary human immunodeficiency virus type 1 infection, J. Virol. 68 (1994) 6103–6110.
[4] T. Matano, R. Shibata, C. Siemon, M. Connors, H.C. Lane, M.A. Martin, Administration of an anti-CD8 monoclonal antibody interferes with the clearance of chimeric simian/human immunodeficiency virus during primary infections of rhesus macaques, J. Virol. 72 (1998) 164–169.
[5] X. Jin, D.E. Bauer, S.E. Tuttleton, S. Lewin, A. Gettie, J. Blanchard, C.E. Irwin, J.T. Safrit, J. Mittler, L. Weinberger, L.G. Kostrikis, L. Zhang, A.S. Perelson, D.D. Ho, Dramatic rise in plasma viremia after CD8(+) T cell depletion in simian immunodeficiency virus-infected macaques, J. Exp. Med. 189 (1999) 991–998.
[6] J.E. Schmitz, M.J. Kuroda, S. Santra, V.G. Sasseville, M.A. Simon, M.A. Lifton, P. Racz, K. Tenner-Racz, M. Dalesandro, B.J. Scallon, J. Ghrayeb, M.A. Forman, D.C. Montefiori, E.P. Rieber, N.L. Letvin, K.A. Reimann, Control of viremia in simian immunodeficiency virus infection by CD8+ lymphocytes, Science 283 (1999) 857–860.
[7] P.J. Goulder, D.I. Watkins, Impact of MHC class I diversity on immune control of immunodeficiency virus replication, Nat. Rev. Immunol. 8 (2008) 619–630.
[8] T. Nomura, T. Matano, Association of MHC-I genotypes with disease progression in HIV/SIV infections, Front. Microbiol. 3 (2012) 234.
[9] S.A. Migueles, M.S. Sabbaghian, W.L. Shupert, M.P. Bettinotti, F.M. Marincola, L. Martino, C.W. Hallahan, S.M. Selig, D. Schwartz, J. Sullivan, M. Connors, HLA B*5701 is highly associated with restriction of virus replication in a subgroup of HIV-infected long term nonprogressors, Proc. Natl. Acad. Sci. U.S.A. 97 (2000) 2709–2714.
[10] T. Muhl, M. Krawczak, P. Ten Haaft, G. Hunsmann, U. Sauermann, MHC class I alleles influence set-point viral load and survival time in simian immunodeficiency virus-infected rhesus monkeys, J. Immunol. 169 (2002) 3438–3446.
[11] M. Altfeld, E.T. Kalife, Y. Qi, H. Streeck, M. Lichterfeld, M.N. Johnston, N. Burgett, M.E. Swartz, A. Yang, G. Alter, X.G. Yu, A. Meier, J.K. Rockstroh, T.M. Allen, H. Jessen, E.S. Rosenberg, M. Carrington, B.D. Walker, HLA alleles associated with delayed progression to AIDS contribute strongly to the initial CD8(+) T cell response against HIV-1, PLoS Med. 3 (2006) e403.
[12] L.J. Yant, T.C. Friedrich, R.C. Johnson, G.E. May, N.J. Maness, A.M. Enz, J.D. Lifson, D.H. O'Connor, M. Carrington, D.I. Watkins, The high-frequency major histocompatibility complex class I allele Mamu-B*17 is associated with control of simian immunodeficiency virus SIVmac239 replication, J. Virol. 80 (2006) 5074–5077.
[13] J.T. Loffredo, J. Maxwell, Y. Qi, C.E. Glidden, G.J. Borchardt, T. Soma, A.T. Bean, D.R. Beal, N.A. Wilson, W.M. Rehrauer, J.D. Lifson, M. Carrington, D.I. Watkins, Mamu-B*08-positive macaques control simian immunodeficiency virus replication, J. Virol. 81 (2007) 8827–8832.
[14] T. Nomura, H. Yamamoto, T. Shiino, N. Takahashi, T. Nakane, N. Iwamoto, H. Ishii, T. Tsukamoto, M. Kawada, S. Matsuoka, A. Takeda, K. Terahara, Y. Tsunetsugu-Yokota, N. Iwata-Yoshikawa, H. Hasegawa, T. Sata, T.K. Naruse, A. Kimura, T. Matano, Association of major histocompatibility complex class I haplotypes with disease progression after simian immunodeficiency virus challenge in Burmese rhesus macaques, J. Virol. 86 (2012) 6481–6490.
[15] T. Matano, M. Kobayashi, H. Igarashi, A. Takeda, H. Nakamura, M. Kano, C. Sugimoto, K. Mori, A. Iida, T. Hirata, M. Hasegawa, T. Yuasa, M. Miyazawa, Y. Takahashi, M. Yasunami, A. Kimura, D.H. O'Connor, D.I. Watkins, Y. Nagai, Cytotoxic T lymphocyte-based control of simian immunodeficiency virus replication in a preclinical AIDS vaccine trial, J. Exp. Med. 199 (2004) 1709–1718.
[16] N.L. Letvin, J.R. Mascola, Y. Sun, D.A. Gorgone, A.P. Buzby, L. Xu, Z.Y. Yang, B. Chakrabarti, S.S. Rao, J.E. Schmitz, D.C. Montefiori, B.R. Barker, F.L. Bookstein, G.J. Nabel, Preserved CD4+ central memory T cells and survival in vaccinated SIV-challenged monkeys, Science 312 (2006) 1530–1533.

[17] N.A. Wilson, J. Reed, G.S. Napoe, S. Piaskowski, A. Szymanski, J. Furlott, E.J. Gonzalez, L.J. Yant, N.J. Maness, G.E. May, T. Soma, M.R. Reynolds, E. Rakasz, R. Rudersdorf, A.B. McDermott, D.H. O'Connor, T.C. Friedrich, D.B. Allison, A. Patki, L.J. Picker, D.R. Burton, J. Lin, L. Huang, D. Patel, G. Heindecker, J. Fan, M. Citron, M. Horton, F. Wang, X. Liang, J.W. Shiver, D.R. Casimiro, D.I. Watkins, Vaccine-induced cellular immune responses reduce plasma viral concentrations after repeated low-dose challenge with pathogenic simian immunodeficiency virus SIVmac239, J. Virol. 80 (2006) 5875–5885.

[18] J. Liu, K.L. O'Brien, D.M. Lynch, N.L. Simmons, A. La Porte, A.M. Riggs, P. Abbink, R.T. Coffey, L.E. Grandpre, M.S. Seaman, G. Landucci, D.N. Forthal, D.C. Montefiori, A. Carville, K.G. Mansfield, M.J. Havenga, M.G. Pau, J. Goudsmit, D.H. Barouch, Immune control of an SIV challenge by a T-cell-based vaccine in rhesus monkeys, Nature 457 (2009) 87–91.

[19] S.G. Hansen, J.C. Ford, M.S. Lewis, A.B. Ventura, C.M. Hughes, L. Coyne-Johnson, N. Whizin, K. Oswald, R. Shoemaker, T. Swanson, A.W. Legasse, M.J. Chiuchiolo, C.L. Parks, M.K. Axthelm, J.A. Nelson, M.A. Jarvis, M. Piatak Jr., J.D. Lifson, L.J. Picker, Profound early control of highly pathogenic SIV by an effector memory T-cell vaccine, Nature 473 (2011) 523–527.

[20] B.H. Edwards, A. Bansal, S. Sabbaj, J. Bakari, M.J. Mulligan, P.A. Goepfert, Magnitude of functional CD8$^+$ T-cell responses to the gag protein of human immunodeficiency virus type 1 correlates inversely with viral load in plasma, J. Virol. 76 (2002) 2298–2305.

[21] R. Zuniga, A. Lucchetti, P. Galvan, S. Sanchez, C. Sanchez, A. Hernandez, H. Sanchez, N. Frahm, C.H. Linde, H.S. Hewitt, W. Hildebrand, M. Altfeld, T.M. Allen, B.D. Walker, B.T. Korber, T. Leitner, J. Sanchez, C. Brander, Relative dominance of Gag p24-specific cytotoxic T lymphocytes is associated with human immunodeficiency virus control, J. Virol. 80 (2006) 3122–3125.

[22] P. Kiepiela, K. Ngumbela, C. Thobakgale, D. Ramduth, I. Honeyborne, E. Moodley, S. Reddy, C. de Pierres, Z. Mncube, N. Mkhwanazi, K. Bishop, M. van der Stok, K. Nair, N. Khan, H. Crawford, R. Payne, A. Leslie, J. Prado, A. Prendergast, J. Frater, N. McCarthy, C. Brander, G.H. Learn, D. Nickle, C. Rousseau, H. Coovadia, J.I. Mullins, D. Heckerman, B.D. Walker, P. Goulder, CD8$^+$ T-cell responses to different HIV proteins have discordant associations with viral load, Nat. Med. 13 (2007) 46–53.

[23] J.A. Borghans, A. Molgaard, R.J. de Boer, C. Kesmir, HLA alleles associated with slow progression to AIDS truly prefer to present HIV-1 p24, PLoS One 2 (2007) e920.

[24] P.A. Mudd, M.A. Martins, A.J. Ericsen, D.C. Tully, K.A. Power, A.T. Bean, S.M. Piaskowski, L. Duan, A. Seese, A.D. Gladden, K.L. Weisgrau, J.R. Furlott, Y.I. Kim, M.G. Veloso de Santana, E. Rakasz, S. Capuano 3rd, N.A. Wilson, M.C. Bonaldo, R. Galler, D.B. Allison, M. Piatak Jr., A.T. Haase, J.D. Lifson, T.M. Allen, D.I. Watkins, Vaccine-induced CD8$^+$ T cells control AIDS virus replication, Nature 491 (2012) 129–133.

[25] N. Iwamoto, N. Takahashi, S. Seki, T. Nomura, H. Yamamoto, M. Inoue, T. Shu, T.K. Naruse, A. Kimura, T. Matano, Control of simian immunodeficiency virus replication by vaccine-induced Gag- and Vif-specific CD8$^+$ T cells, J. Virol. 88 (2014) 425–433.

[26] M. Kawada, T. Tsukamoto, H. Yamamoto, N. Iwamoto, K. Kurihara, A. Takeda, C. Moriya, H. Takeuchi, H. Akari, T. Matano, Gag-specific cytotoxic T-lymphocyte-based control of primary simian immunodeficiency virus replication in a vaccine trial, J. Virol. 82 (2008) 10199–10206.

[27] T. Tsukamoto, A. Takeda, T. Yamamoto, H. Yamamoto, M. Kawada, T. Matano, Impact of cytotoxic-T-lymphocyte memory induction without virus-specific CD4+ T-Cell help on control of a simian immunodeficiency virus challenge in rhesus macaques, J. Virol. 83 (2009) 9339–9346.

[28] H. Ishii, M. Kawada, T. Tsukamoto, H. Yamamoto, S. Matsuoka, T. Shiino, A. Takeda, M. Inoue, A. Iida, H. Hara, T. Shu, M. Hasegawa, T.K. Naruse, A. Kimura, M. Takiguchi, T. Matano, Impact of vaccination on cytotoxic T lymphocyte immunodominance and cooperation against simian immunodeficiency virus replication in rhesus macaques, J. Virol. 86 (2012) 738–745.

[29] J.R. Arguello, A.M. Little, A.L. Pay, D. Gallardo, I. Rojas, S.G. Marsh, J.M. Goldman, J.A. Madrigal, Mutation detection and typing of polymorphic loci through double-strand conformation analysis, Nat. Genet. 18 (1998) 192–194.

[30] T.K. Naruse, Z. Chen, R. Yanagida, T. Yamashita, Y. Saito, K. Mori, H. Akari, Y. Yasutomi, M. Miyazawa, T. Matano, A. Kimura, Diversity of MHC class I genes in Burmese-origin rhesus macaques, Immunogenetics 62 (2010) 601–611.

[31] M. Kawada, H. Igarashi, A. Takeda, T. Tsukamoto, H. Yamamoto, S. Dohki, M. Takiguchi, T. Matano, Involvement of multiple epitope-specific cytotoxic T-lymphocyte responses in vaccine-based control of simian immunodeficiency virus replication in rhesus macaques, J. Virol. 80 (2006) 1949–1958.

[32] B.R. Mothe, J. Sidney, J.L. Dzuris, M.E. Liebl, S. Fuenger, D.I. Watkins, A. Sette, Characterization of the peptide-binding specificity of Mamu-B*17 and identification of Mamu-B*17-restricted epitopes derived from simian immunodeficiency virus proteins, J. Immunol. 169 (2002) 210–219.

[33] M.L. Budde, J.M. Greene, E.N. Chin, A.J. Ericsen, M. Scarlotta, B.T. Cain, N.H. Pham, E.A. Becker, M. Harris, J.T. Weinfurter, S.L. O'Connor, M. Piatak Jr., J.D. Lifson, E. Gostick, D.A. Price, T.C. Friedrich, D.H. O'Connor, Specific CD8$^+$ T cell responses correlate with control of simian immunodeficiency virus replication in Mauritian cynomolgus macaques, J. Virol. 86 (2012) 7596–7604.

OPEN ACCESS Freely available online

PLOS ONE

HIV-1 Vpr Induces Interferon-Stimulated Genes in Human Monocyte-Derived Macrophages

Muhammad Atif Zahoor[1,2☯], Guangai Xue[1,2☯], Hirotaka Sato[1], Tomoyuki Murakami[1], Shin-nosuke Takeshima[1], Yoko Aida[1]*

1 Viral Infectious Diseases Unit, RIKEN, Wako, Saitama, Japan, **2** Japanese Foundation of AIDS Prevention, Tokyo, Japan

Abstract

Macrophages act as reservoirs of human immunodeficiency virus type 1 (HIV-1) and play an important role in its transmission to other cells. HIV-1 Vpr is a multi-functional protein involved in HIV-1 replication and pathogenesis; however, its exact role in HIV-1-infected human macrophages remains poorly understood. In this study, we used a microarray approach to explore the effects of HIV-1 Vpr on the transcriptional profile of human monocyte-derived macrophages (MDMs). More than 500 genes, mainly those involved in the innate immune response, the type I interferon pathway, cytokine production, and signal transduction, were differentially regulated (fold change >2.0) after infection with a recombinant adenovirus expressing HIV-1 Vpr protein. The differential expression profiles of select interferon-stimulated genes (ISGs) and genes involved in the innate immune response, including *STAT1, IRF7, MX1, MX2, ISG15, ISG20, IFIT1, IFIT2, IFIT3, IFI27, IFI44L, APOBEC3A, DDX58* (RIG-I), *TNFSF10* (TRAIL), *and RSAD2* (viperin) were confirmed by real-time quantitative PCR and were consistent with the microarray data. In addition, at the post-translational level, HIV-1 Vpr induced the phosphorylation of STAT1 at tyrosine 701 in human MDMs. These results demonstrate that HIV-1 Vpr leads to the induction of ISGs and expand the current understanding of the function of Vpr and its role in HIV-1 immune pathogenesis.

Citation: Zahoor MA, Xue G, Sato H, Murakami T, Takeshima S-n, et al. (2014) HIV-1 Vpr Induces Interferon-Stimulated Genes in Human Monocyte-Derived Macrophages. PLoS ONE 9(8): e106418. doi:10.1371/journal.pone.0106418

Editor: Wenzhe Ho, Temple University School of Medicine, United States of America

Received June 11, 2014; **Accepted** August 6, 2014; **Published** August 29, 2014

Data Availability: The authors confirm that all data underlying the findings are fully available without restriction. Microarray data have been deposited in NCBI's Gene Expression Omnibus and assigned the GEO Series accession number GSE56591. All relevant data are within the paper.

Funding: This work was supported by a Health Sciences Research Grant from the Ministry of Health, Labor and Welfare of Japan, Research on HIV/AIDS: (http://www.jhsf.or.jp/English/index_e.html) and the Japan Society for the Promotion of Science (JSPS) Postdoctoral Fellowship for Foreign Researchers (http://www.jsps.go.jp/english/e-fellow/postdoctoral.html). The funders had no role in study design, data collection and analysis, the decision to publish, or the preparation of the manuscript.

Competing Interests: The authors have declared that no competing interests exist.

* Email: aida@riken.jp

☯ These authors contributed equally to this work.

Introduction

Antigen-presenting cells (APCs) are critical for both innate and adaptive immunity. Professional APCs such as macrophages play an integral role in the immune pathogenesis of the human immunodeficiency virus type 1 (HIV-1) [1]. HIV-1 is a member of the lentivirus family and is the etiologic agent of acquired immunodeficiency syndrome (AIDS). It interacts with host cells through multiple signaling pathways to establish the disease [2]. The infection involves complex mechanisms through which HIV-1 overcomes the host immune responses and causes reprogramming of the host transcriptome and proteome [3–5].

Vpr, an accessory gene product of HIV-1, is a protein of 96 amino acids and has a predicted molecular weight of 15 kDa that is relatively conserved in HIV-1 and simian immunodeficiency virus (SIV) [6]. Vpr is a pleiotropic protein that is involved in diverse functions including cell-cycle arrest at the G2/M phase [7], apoptosis [7–9], nuclear import of the pre-integration complex [10–14], transcriptional activation [15], and splicing [16,17]. Vpr performs these functions through interactions with various host cellular factors such as DCAF1, SAP145, p300, and importin-α [8,10,11,12,16,18–21].

A striking feature of Vpr is its unique potential to promote viral productivity in monocytes/macrophages and in a small population of $CD4^+$ T-cells [22–26]. Although Vpr is thought to play an important role in HIV-1-infected human macrophages [1,3,6,11,21,23], little is known about how it disrupts the expression profile of host cellular genes. In this study, we analyzed the effect of Vpr on the expression profiles of host cellular genes in human monocyte-derived macrophages (MDMs), with the idea that such an analysis would provide useful information about the involvement of genes not yet identified through biochemical approaches. Human MDMs were generated from peripheral blood mononuclear cells (PBMCs) and infected with a recombinant adenovirus expressing Vpr, and analyzed by cDNA microarray. HIV-1 Vpr protein induced interferon (IFN)-stimulated genes (ISGs) such as *IRF7*, and caused phosphorylation of STAT1 at tyrosine 701 in human MDMs. These findings enhance the current understanding of HIV-1 replication and pathogenesis in human macrophages.

Results

Expression of Vpr and ZsGreen1 in human MDMs

To better understand the role of HIV-1 Vpr protein in human MDMs, a recombinant adenovirus expressing ZsGreen1 and FLAG-tagged Vpr, Ad-Vpr, was generated. As a control, a recombinant adenovirus expressing ZsGreen1, Ad-Zs, was used. A schematic diagram of both recombinant adenoviruses is shown in Figure 1A. To examine whether Vpr induces cell-cycle arrest at the G2 phase, HeLa cells were infected with Ad-Vpr or Ad-Zs at a multiplicity of infection (MOI) of 50. At 48 h post-infection, cells were harvested for analysis of DNA content and stained with propidium iodide (PI). The DNA content of ZsGreen1-positive cells was analyzed by flow cytometry, which revealed a dramatic increase in the proportion of cells in the G2 phase of the cell cycle in cells infected with Ad-Vpr (21.22% and 70.37% were in the G1 and the G2+M phases, respectively, and the G2+M: G1 ratio was 3.32) compared to cells infected with the control Ad-Zs (54.06% and 23.87% were in the G1 and G2/M phases, respectively, and the G2+M: G1 ratio was 0.44) (Figure 1B). These results indicate that the recombinant adenovirus expressing FLAG-Vpr induces G2 cell-cycle arrest.

Purified and titrated Ad-Vpr and Ad-Zs were next used to infect MDMs derived from peripheral blood monocytes from two normal healthy donors (Figure 2). PBMCs were isolated from heparinized whole blood from two healthy donors by standard density gradient centrifugation with Ficoll-Paque. PBMCs were harvested from the interface and $CD14^+$ cells were separated by high-gradient magnetic sorting using MACS beads. The isolated $CD14^+$ cells were differentiated into MDMs for 7 days, and then infected with the Ad-Vpr or Ad-Zs at a MOI of 100. After 48 h, the cells were either observed under a fluorescence microscope or lysed and analyzed for the expression of Vpr and ZsGreen1 protein by Western blotting. Fluorescence microscopy showed that ZsGreen1 was expressed in both Ad-Vpr- and Ad-Zs-infected MDMs compared to mock-infected controls, which remained ZsGreen1-negative (Figure 2A). As shown in Figure 2B, a 26 kDa band representing ZsGreen1 and a 14 kDa band representing Vpr was detected; these apparent molecular masses are consistent with their respective predicted sequences. Further, there was no difference in ZsGreen1 expression between the two populations of MDMs (Figure 2B). These results confirm the suitability of the adenovirus-infected MDMs for downstream assays.

Microarray analysis of MDMs infected with Ad-Vpr or Ad-Zs

To evaluate changes in the expression of host cellular genes in response to HIV-1 Vpr protein, Ad-Vpr- and Ad-Zs-infected macrophages were subjected to cDNA microarray analyses using a commercially available Affymetrix GeneChip oligonucleotide array (Human Genome U133 Plus 2.0), which interrogates more than 47,000 transcripts from 38,500 genes. This approach enabled us to monitor Vpr-induced changes in the global gene profile of the MDMs. Data analysis using GeneSpring GX software showed that Vpr modulated the expression of 557 genes in Donor 1 and 116 genes in Donor 2. Given that the array analyzes more than 47,000 gene transcripts, this is considered a minor change in the global host gene profiles (Figure 3). Heat maps from both donors (Figure 3) show that the global gene expression profiles were different in each donor, indicating that there is individual variability in the response to Vpr at the transcriptional level.

The differentially regulated genes were filtered to determine gene entities common to both donors. Out of 557 genes altered in response to Vpr in Donor 1 and 116 genes in Donor 2, only 66

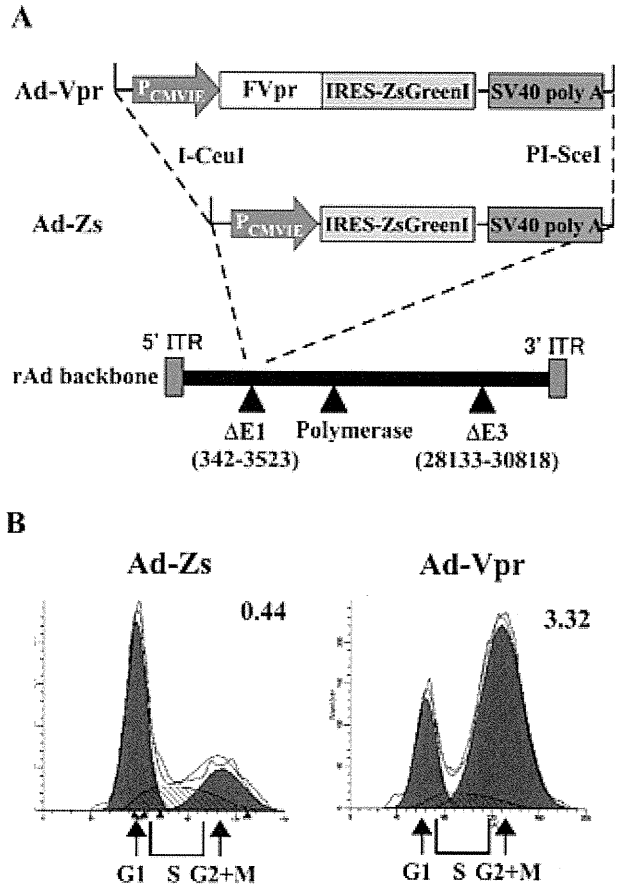

Figure 1. Schematic diagram of the Ad-Vpr and Ad-Zs vectors and analysis of their functional expression. (A) Recombinant adenovirus vectors expressing either FLAG-Vpr and ZsGreen1 or ZsGreen1 were generated using the Adeno-X™ expression system, as described in Materials and Methods. The transgene cassettes that replace the deleted E1 region contain a cytomegalovirus (CMV) promoter driving the expression of FLAG-Vpr and ZsGreen1 or ZsGreen1 protein, followed by an SV40 polyadenylation signal. The solid triangles indicate the regions deleted in the recombinant adenovirus (rAd) backbone. ITR: Inverted terminal repeats. (B) HeLa cells were infected with Ad-Vpr or Ad-Zs at MOI 50. At 48 h post-infection, cells were fixed and stained with propidium iodide for the analysis of DNA content. ZsGreen1-positive cells were analyzed by flow cytometry using Cell Quest for acquisition and ModFit LT. Arrowheads indicate peaks representing cells in the G1 and G2+M phases. The G2+M: G1 ratio is indicated in the upper right of each graph.
doi:10.1371/journal.pone.0106418.g001

genes were common to both (Figure 4A). Gene ontology was ranked based on the corrected p-values. The ten most significant pathways common to both donors are shown in Figure 4B. HIV-1 Vpr significantly altered the expression profiles of cellular genes mainly involved in the innate immune response, type I IFN signaling, and cytokine-mediated signaling. A complete list of all 66 genes common to both donors is shown in the form of heat maps in Figure 4C.

Most of the altered genes were involved in the immune response or the defense response (Figure 4B); therefore, genes related to the immune response (GO: 0006955) were further analysed. A complete list of the 126 and 41 genes differentially regulated in Donor 1 and Donor 2 respectively, is shown in Table 1. A significant majority of the up-regulated genes are involved in the immune response. *IFI44L* (40-fold), *CXCL10* (23-fold), *MX1* (15-

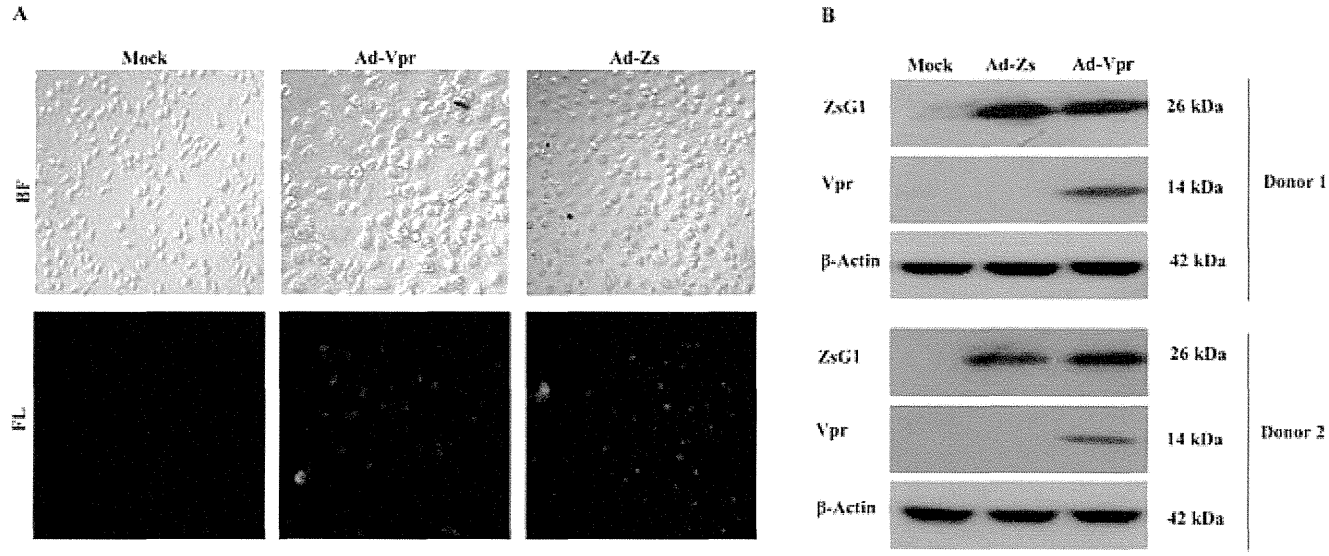

Figure 2. Expression analyses of HIV-1 Vpr protein in human monocyte-derived macrophages (MDMs). (A) Peripheral blood mononuclear cells (PBMCs) were isolated from two healthy donors through leukophoresis, cultured *in vitro*, and differentiated into MDMs as described in Materials and Methods. At day 7, the MDMs were infected with either Ad-Vpr or Ad-Zs, or were left untreated as mock-infected controls (left). At 48 h post-infection, the cells from Donor 1 were visualized by fluorescence (FL) and bright field phase contrast (BF) microscopy. (B) The cells from the two donors (upper panel, Donor 1; lower panel, Donor 2) were lysed and subjected to Western blot analyses using Vpr, ZsGreen1, and β-actin antibodies.
doi:10.1371/journal.pone.0106418.g002

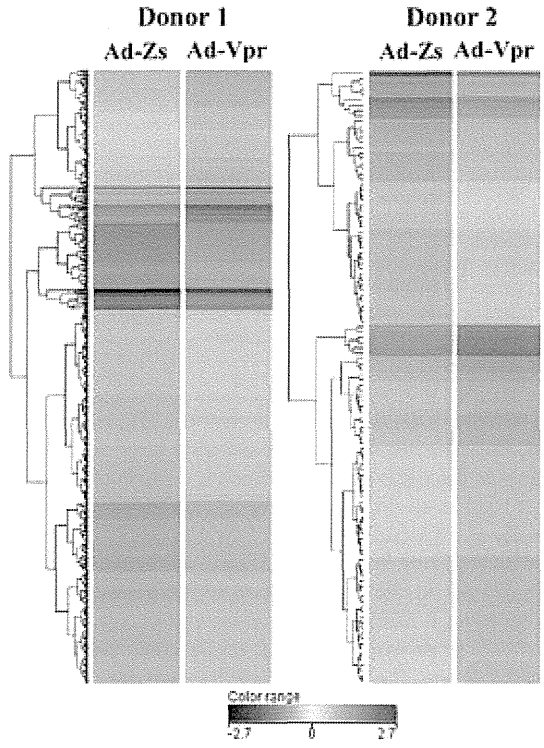

Figure 3. Differential expression profiling of cellular genes after infection with Ad-Vpr in human monocyte-derived macrophages (MDMs). Heat map of hierarchical gene clustering showing all genes that were either up- or down-regulated (>2-fold change) upon Ad-Vpr infection in MDMs from both donors. The color represents the normalized expression of genes in MDMs infected with Ad-Vpr or Ad-Zs (see color key). Gene up-regulation is denoted in red and gene down-regulation is denoted in blue.
doi:10.1371/journal.pone.0106418.g003

fold), *CCL8* (13-fold), *IFIT1* (10-fold), *TNFSF10* (TRAIL) (8-fold), *ISG20* (8-fold), *IFIT2* (8-fold), *APOBEC3A* (7-fold), *CXCL11* (7-fold), *IFI27* (7-fold), *OAS2* (7-fold), *IRF7* (6-fold), and *ISG15* (5-fold) were the most highly up-regulated genes, whereas *PPBP*(CXCL7) (96-fold), *MARCO* (13-fold), *CXCL5* (7-fold), *MT2A* (6-fold), and *CCL22* (4-fold) were the most highly down-regulated genes in Donor 1 (Table 1). In contrast, *IFI44L* (12-fold), *MX1* (7-fold), *APOBEC3A* (6-fold), *IFIT1* (5-fold), *IFIT2* (4.5-fold), *IFIT3* (4-fold), *ISG15* (3-fold), *XAF1* (3-fold), *OAS3* (3-fold), *CCL8* (3-fold), *OAS2* (3-fold), *DDX58* (2.5-fold), *STAT1* (2-fold), *MX2* (2-fold), *IRF7* (2-fold) and *CCL2* (2-fold) were the most highly up-regulated genes, whereas *THBS1* (3-fold), *HLA-DQA* (3-fold), *TLR7* (2.6-fold), *CD74* (2.5-fold), *CXCL2* (2-fold), *CCR2* (2-fold) and *CXCL9* (2-fold) were the most highly down-regulated genes in Donor 2 (Table 1). By close examination of the data set (Figure 5 and Table 1), it was observed that several ISGs, which are mainly produced in response to type I interferon [27], were up-regulated in the Vpr-expressing MDMs. A hierarchical heat map of all the genes up-regulated in Donor 1 (>2.0-fold change) that are related to the immune response and type 1 IFN signalling is shown in Figure 5A and B. Collectively, microarray analyses indicate that HIV-1 Vpr leads to the differential regulation of genes involved in innate immunity, type I IFNs, cytokine production, and cell signalling, resulting in activation of antiviral responses in MDMs.

Validation of the expression of host genes involved in the type 1 IFN pathway by real-time quantitative reverse transcription-polymerase chain reaction (qRT-PCR)

Validation of the results obtained by microarray analysis was performed by qRT-PCR evaluating the mRNA levels of selected up-regulated genes involved in the immune response. Genes were selected for confirmation either because they were known to be induced in response to type I IFN and reportedly involved in the innate immune antiviral response [27,28] or because they were